11th ANKARA INTERNATIONAL AEROSPACE CONFERENCE **AIAC-2021-081**
8-10 September 2021 - METU, Ankara TURKEY

IDENTIFICATION OF AERODYNAMIC CHARACTERISTICS OF GENERIC UCAV CONFIGURATIONS FOR LOW-SPEED FLOWS

Hassan Aleisa[1] and Konstantinos Kontis[2]
University of Glasgow
Glasgow, Scotland

Melike Nikbay[3]
Istanbul Technical University
Istanbul, Turkey

ABSTRACT

The present work discusses the flow progression and the aerodynamic characteristics of generic unmanned combat aerial vehicle (UCAV) models at various angles of attack. The geometry models used for numerical simulations were created in SolidWorks. The open-source software such as Salome and SnappyHexMesh were used for generating the grid, and OpenFOAM was used to compute the aerodynamics characteristics of the different wing models. Later, the numerical results were validated against the experimental data available in the open literature. The present computational results showed good agreement with the experimental values, thereby validating the accuracy of the present methodology to predict the aerodynamic characteristics of the UCAV wing models.

INTRODUCTION

Understanding the aerodynamic characteristics of swept flying wings at moderate to higher angles of attack (AOA) is essential for the UCAVs' enhanced performance and maneuverability. The flying wing types are dominated by delta and lambda wing configurations, as the use of delta or lambda wing enhances the performance of UCAVs at high AOA. The flow over the delta wing produces vortices because of the separated flow over the leading edge (LE) of a delta wing at a non-zero AOA. These vortices result in lower pressure regions and may reach thirty percent of the entire lift at medium AOA [Puckett and Stewart, 1947]. However, the benefits obtained by the swept flying wing vortices are limited; at a higher AOA, the vortex breakdowns result in an abrupt reduction in the lift due to stall condition. Generally, all wing types experience separated flow at high AOA by cause of the viscous influences. However, the swept-wing configurations which adopted sharp LE are significantly influenced by LE flow separation. The LE vortices influence the performance of the UACV significantly at moderate to higher AOA values.

[1] PhD student in Aerospace Engineering Department, School of Engineering, University of Glasgow, Email: 2501058A@student.gla.ac.uk
[2] Professor in Aerospace Engineering Department, School of Engineering, University of Glasgow, Email: kostas.kontis@glasgow.ac.uk
[3] Professor in Astronautical Engineering Department, Faculty of Aeronautics and Astronautics, Istanbul Technical University, AeroMDO Lab. Email: nikbay@itu.edu.tr

Lambourne and Bryer (1959) performed an experimental investigation of vortex flow separation on a 65° sweepback wing with a sharp LE. They concluded a favorable pressure gradient through the vortex core, and the axial velocity through the vortex flow is greater than the far-field velocity and raises significantly as it advances towards the axis center. Lambourne and Bryer (1961) also studied the vortex breakdown behavior employing flow visualization methods. This study reported that the vortex breakdown could be occurred due to the combined effect of reduced total pressure and unfavorable pressure gradient through the vortex axis. Elsewhere, Earnshaw (1961) studied the sharp LE on a delta wing that generated a primary vortex and differentiated it into viscous subcore, rotational core, and free shear layer. Polhamus (1971) developed the leading-edge suction analogy applied to wings with adequate sharp LEs, which exhibits separation at the LE. Many investigations were carried out to analyze the vortex flow by conducting wind tunnel experiments [Canpolat *et al.*, 2012; Sidorenko *et al.*, 2013; Manshadi *et al.*, 2016; Zhang *et al.,* 2019] and computational fluid dynamics (CFD) [Verhaagen, 2011; Abd Halim and Mat, 2015; Wibowo *et al.,* 2018]. These studies predicted the aerodynamic characteristics of wings with fixed aspect ratio, LE sweep angles, and varied LE contours.

Recent flying wings research has been motivated to understand the complex flow structures of various UCAV configurations such as lambda and delta wings with moderate and high sweep angles. Moreover, the UCAV models such as the 1303 and the SACCON were developed and studied to understand their aerodynamics characteristics [Petterson, 2006; Patel *et al.,* 2007; Frink, 2010; Huber *et al*., 2012; Shima and Parka, 2013]. However, varying sweep angles are adopted in UCAV designs such as the Boeing X-45 and the Northrop Grumman X-47B, combined with different trailing edge configurations, provide distinctive flow features compared to the simple delta or lambda wing models. The critical parameters that influence the flow behavior are the AOA, LE shape, wing planform, and sweep. Generally, at a higher AOA, sharp LEs are preferred because of their maneuverability and low observability [Hövelmann, 2016].

For the slender wing configurations, the strength of the LE vortex increases with a decrease in the sweep, and the vortex breakdowns at a low AOA value. Likewise, an appropriate combination of highly swept inboard and low swept outboard for different wing shapes can enhance the aerodynamic characteristics. To understand the flow behaviour of such configuration, the present work numerically investigates the aerodynamic characteristics of various types of UCAV wing models using OpenFOAM 5.0. The sharp-edged delta and lambda wings with constant and non-constant LE sweep angles are involved in this study. Their flow field analyses are reported using the post-processed figures. The structure of the present work is divided into sections such as numerical methodology, results, and discussion, followed by the conclusion.

NUMERICAL METHODOLOGY

The current investigation involves a computational study to obtain the aerodynamic loads for the 65^o delta, 65^o/40^o double-delta, 40^o lambda, and 65^o/40^o cranked lambda wing models. The various model with specifications, as shown in Table 1, are considered for the validation analysis.

Table 1: Key features of the wing models

Parameters/Configurations	Delta wing		Lambda wing	
Leading-edge/inboard sweep, $\Lambda_{le}=\Lambda_i$ (^{o})	65^o	65^o	40^o	65^o
Outboard sweep, Λ_o, (^{o})	-	40^o	-	40^o
Trailing edge sweep, (^{o})	-	-	40^o	40^o
Root chord, cr, (*m*)	0.320	0.300	0.250	0.360
Wing area, S, (m^2)	0.050	0.055	0.060	0.070
Aspect Ratio, AR, (-)	1.800	4.00	3.780	3.250
Thickness, t, (*m*)	0.006			
Bevel angle (^{o})	6^o			

Grid generation

To exploit the symmetric nature of the wing model, the half span of the model with symmetric boundary conditions is used for the present computations. The CAD models are produced using *SolidWorks 2016* and then exported to a grid generator as STEP and STL files. The open-source grid generators, namely *Salome* and *blockMesh+snappyHexMesh,* are used to discretize the computational flow domain.

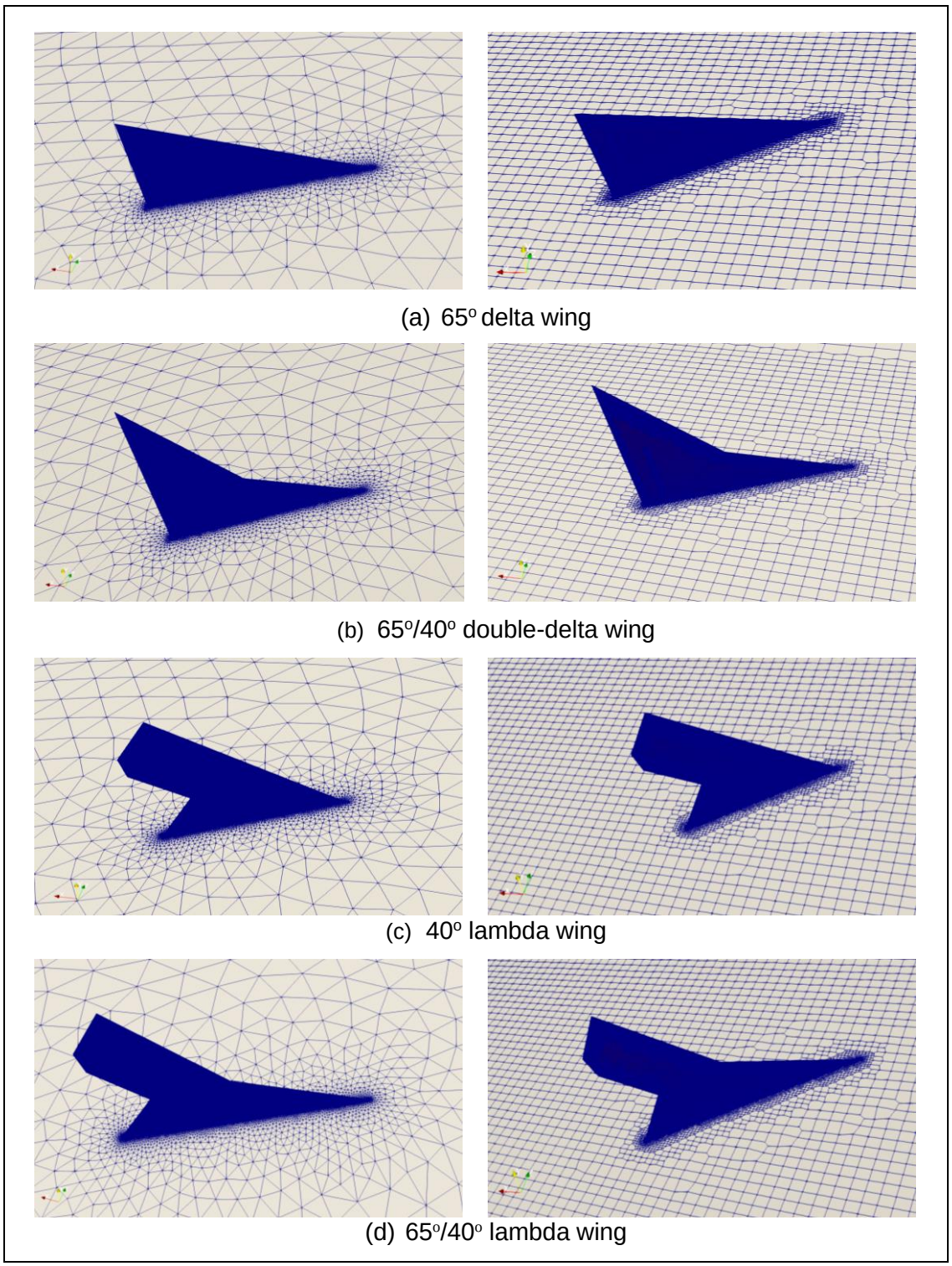

(a) 65^{o} delta wing

(b) 65^{o}/40^{o} double-delta wing

(c) 40^{o} lambda wing

(d) 65^{o}/40^{o} lambda wing

Figure 1: Grids for various UCAV models using Salome (left) and snappyHexMesh (right)

The mesh details of the wing models are provided in Table 2.

Table 2: Mesh details of the wing models

Model	No. of Elements (Million cells)
65^o delta wing	1.809 – 2.242
65/40^o double-delta wing	1.793 – 2.495
40^o lambda wing	1.930 – 3.184
65 ^{o}/40^o lambda wing	2.527 – 3.789

The meshing options used for this study are Salome and cfMesh (independent), blockMesh, and SnappyHexMesh (inbuilt in OpenFOAM). Each mesh generator has its advantages and disadvantages. For simple geometries, the blockMesh is an ideal choice of grid generator; however, it has a steep learning curve, and it is not easy to generate mesh for complex geometries. The blockMesh is a good option if the geometry is easily represented by a reasonable number of points and curves. It is used to generate the background mesh for the snappyHexMesh.

Regarding the grid generator Salome (version 9.6.0), it offers both structured and unstructured meshes. In the present study, the combination of tetrahedral elements with prism layers was tried first. However, due to the sharp edges of the wing configurations, the Salome produced pyramid elements which created a problem in the export of mesh to OpenFOAM. The mesh generated in Salome should be exported as UNV format, and it cannot save the pyramid elements. Hence the present study used fully tetrahedral mesh with no prism elements due to this limitation (Figure 1).

The snappyHexMesh uses the background mesh generated from the blockMesh as the input. It requires the background mesh and the STL file of the wing configurations to generate the mesh. It produces 3D mesh involving hexahedral, polyhedral, and prism cells from a triangulated surface geometry in STL format (Figures 1 and 2). The snappyHexMesh offers various options to refine the edges, surfaces, and volumes to generate a better mesh. The main limitation of the snappyHexMesh is its inability to generate higher-quality prism layers for resolving the viscous sub-layer region. Generally, the prism layers collapse in some regions of the sharp edges, and it is not evenly distributed. A similar problem was faced by various authors who used snappyHexMesh [Ashton *et al.*, 2018] as their grid generator.

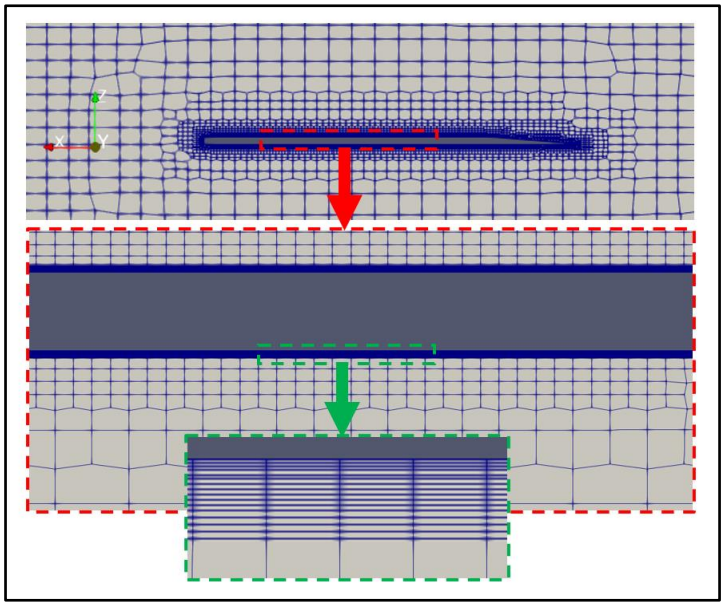

Figure 2: The view of grids and prism layers on the models using SnappyHexMesh

y+ distribution

Identical grid generation inputs are used for the different geometries; however, their features led to some variation in the final grids. To maintain the y+ <1, 15 prism layers are generated on the wing model with a layer growth ratio of 1.05. Figure 3 represents the suction side (SS) y+ distribution for the various wing models.

As illustrated in the figure, for all cases, the value of y+ lies between 0 and 2.5. The maximum value of y+ of 2.5 occurs at the sharp edges of the leeward beveled LE, and y+ ≤ 1.6 occurs at the most surface of the beveled LE. The majority of SS and the pressure side (PS) shows y+ ≤ 1.0. Therefore, the conclusion can be drawn that the present mesh sufficiently resolves the boundary layer for all the wing models analyzed in this study.

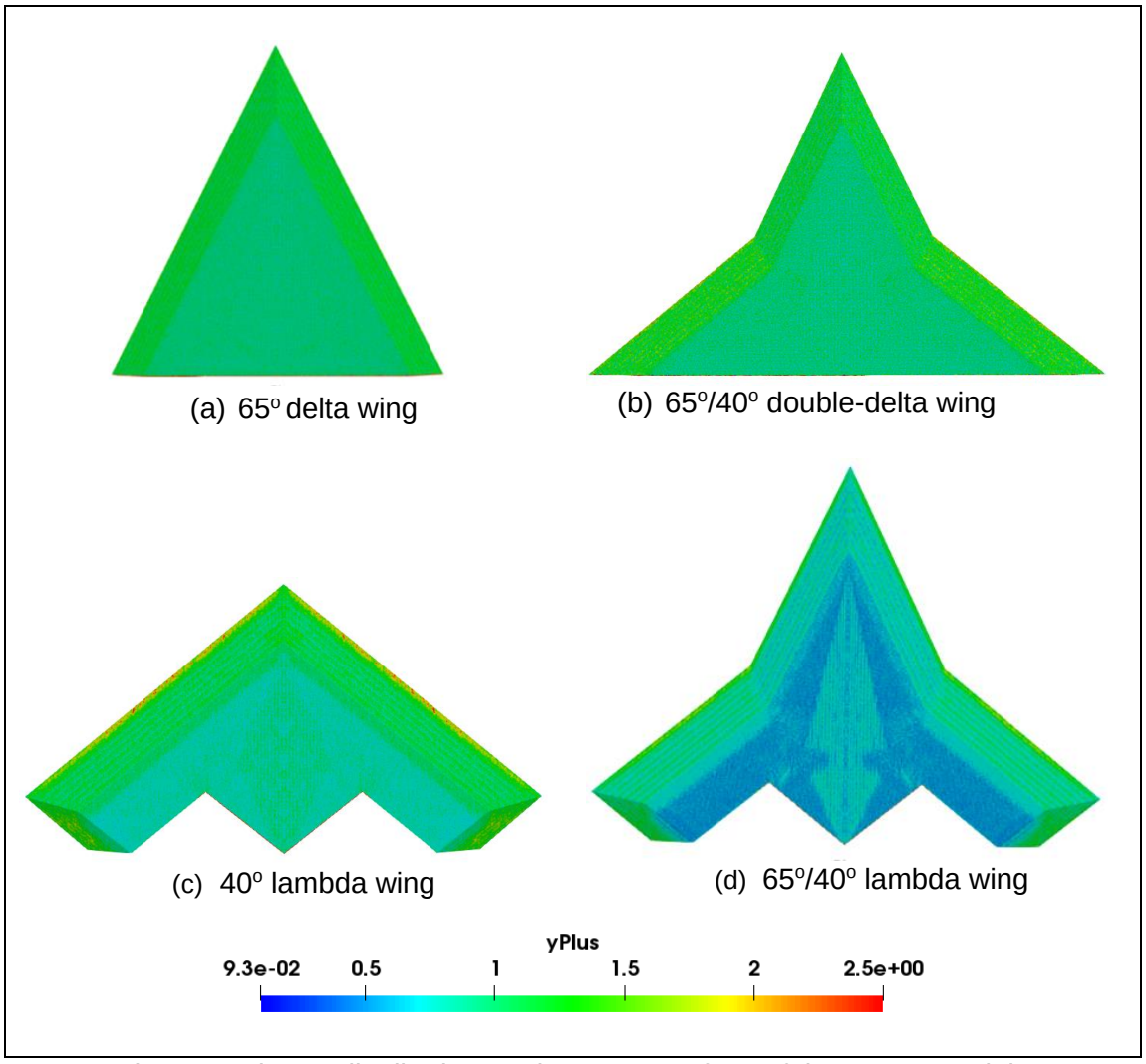

Figure 3: The y+ distribution on the upper surface of the UCAV models

Solver

OpenFOAM 5.0 [Greenshields, 2015] is used to perform numerical simulations to obtain the aerodynamic characteristics of the various wing models analyzed in this work. The flow is analyzed around the wing at Mach number, M = 0.04, and AOA ranged from 0° – 40° with the step of 5°. The OpenFOAM offers various solvers, and based on the present problem, the simpleFOAM solver is chosen for the analyses.

Turbulence Model

Regarding the selection of turbulence models, the present study includes the results of realizable k-ε and the k-ω shear stress transport (SST) models. The realizable k-ε is an improved form of the k-ε model, which has the eddy viscosity coefficient dependent on local flow parameters.

On the contrary, the k-ω SST model is a hybrid model which uses k-ω in the region closer to the wall and k-ε in the region away from the wall. Moreover, proper y+ values are maintained to satisfy the requirements of the turbulence model. The specifications of the numerical study, such as the boundary conditions, gradient, divergence schemes, and flow domain, etc., are provided in Table 3. Additionally, the under-relaxation factors are provided to improve the convergence of the numerical simulations (Table 4).

Table 3 Specifications of numerical study

Working fluid	Air
Type of analysis	Steady
Nature of flow	Incompressible
Computational domain	Half span with symmetry plane.
Mach number (M)	0.04
Outlet	Zero gradient
Wing	No-slip wall
Top, bottom, and side faces	Slip wall
Lateral face	Symmetry plane
Turbulence intensity	5%
Turbulence model	Realizable k-ε and k-ω SST
gradSchemes	Gauss linear
divSchemes	bounded Gauss upwind
Residual convergence	1E-6

Table 4 Under-relaxation factors.

Pressure (p)	0.5
Velocity (U)	0.7
Turbulent kinetic energy (k)	0.7
Omega (ω)	0.7

RESULTS AND DISCUSSION

The present numerical investigation compares lift and drag values for various generic UCAV flying wings using OpenFOAM. Four flying wing models with a baseline configuration have been chosen for CFD analysis.

Numerical validation

The predicted computational lift and drag coefficients are compared with the experimental works of Al-Garni *et al*., 2008 (delta wing), and Patel *et al.*, 2007 and Ali and Chadwick, 2016 (lambda wing). Figure 4 shows the experimental and CFD results comparison of lift coefficient (C_L) data for 65^o delta and 65^o/40^o delta wing. The lift and drag values are compared against the AOA ranging from 0^o to 40^o. As evident in the figure, with an increase in AOA, the C_L increases up to a certain AOA until the stall occurs and then drops gradually. The present numerical C_L values match closely with the experimental values up to AOA = 30^{o,} and at a higher AOA value, it deviates because of possible stall inception in the numerical models. Regarding the drag coefficient (C_D), the variation at the higher AOAs is less pronounced.

Figure 5 shows a comparison of experiments and CFD values of C_L for 40º and 65º/40º lambda wings. The numerical results match well with the experimental values throughout the entire flow range. The stall point of the 40º and 65º/40º lambda wings are 20º and 30º, respectively. The CFD results match relatively well at the post-stall condition compared to the results of the delta wing.

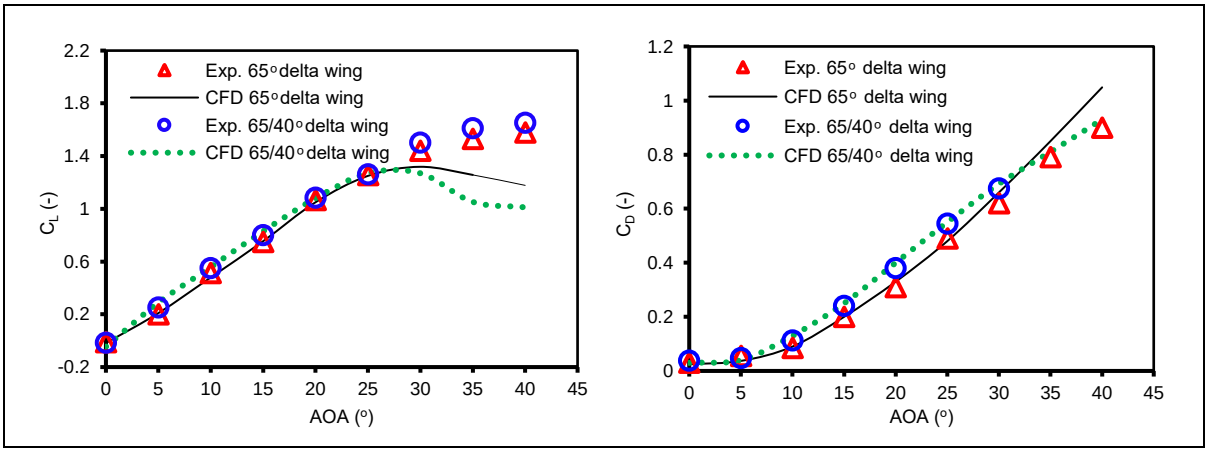

Figure 4: CFD validation with experimental data for 65º and 65º/40º delta wings

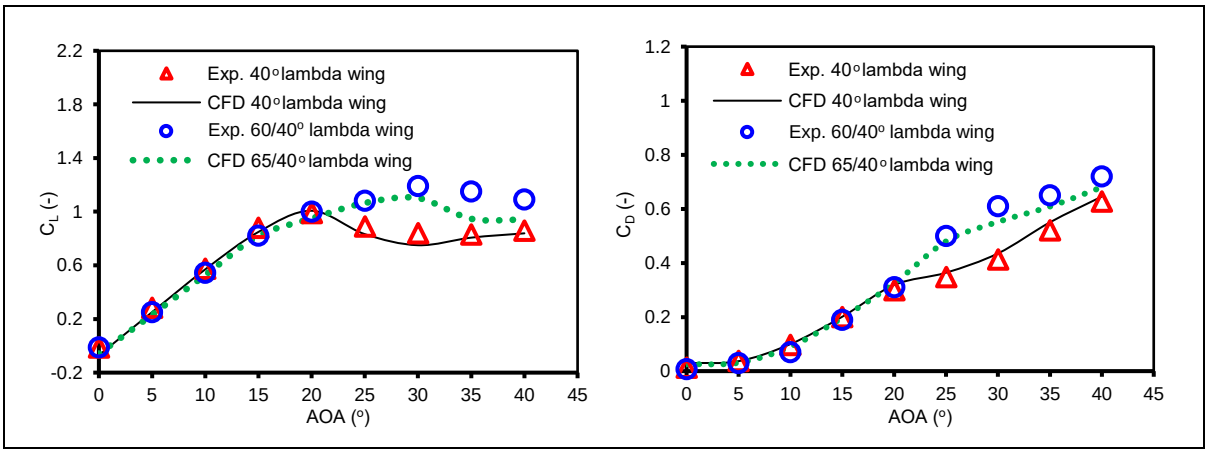

Figure 5: CFD validation with experimental data for 40º and 65º/40º lambda wings

The sweep angle of the wing significantly influences the aerodynamic characteristics of the swept-wing configurations. The flow physics of swept-wing is influenced by wing characteristics such as LE geometry and thickness. At the same angle of attack, the breakdown location of the LE vortex is delayed for leeward beveled and double-beveled compared to windward beveled. The leeward beveled LE improves the lift, stalling characteristic, and the lift-to-drag ratio compared to the double-beveled and windward beveled [Wang and Zhan, 2005]. Hence, in this study, the leeward beveled LE is used for the four configurations.

Flowfield analyses

Figures 6 - 8 display the non-dimensional velocity magnitude distribution for the four wing models at 15º, 20º, and 25º AOA. These specific AOA values lie moderate to the high regime and show better agreement with the experimental results. Figure 6 provides the non-dimensional velocity comparison between the 65º and 65º/40º delta wings for different AOA values. At AOA = 15º, the velocity distribution for the 65º and 65º/40º delta wings shows similar behavior. However, the 65º/40º delta wing exhibits an increased velocity on the SS due to the influence of strakes. The stagnation point occurs on the PS, and the flow accelerates to the SS. The flow experiences an adverse pressure gradient as it approaches the trailing edge (TE) and separates near the TE.

As shown in the figure, the phenomenon mentioned above becomes more pronounced with an increase in AOA, and the 65º/40º delta wing displays relatively increased velocity compared to the 65º delta wing. Moreover, the flow separation is restricted to the small region in the TE for all cases, as the AOA values compared here are lesser than the critical AOA value.

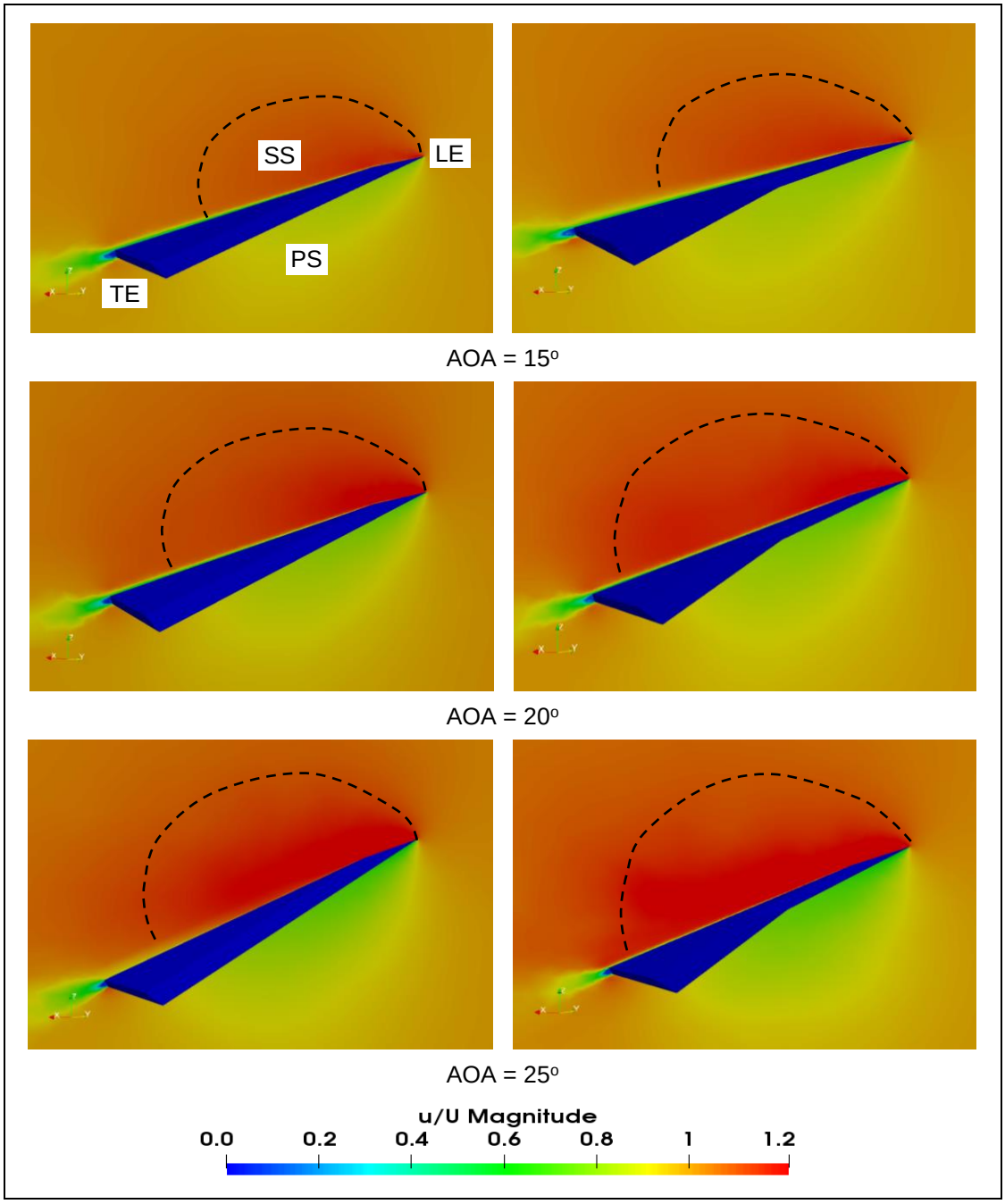

Figure 6: Non-dimensional velocity magnitude of 65º and 65º/40º delta wings

The non-dimensional velocity distribution of the 40º and 65º/40º lambda wings at different AOA values (Figure 7). At AOA = 15º, the 40º lambda wing shows relatively higher velocity on the SS than the 65º/40º lambda wing because of the increased wing loading. This effect becomes more pronounced with the increase in AOA (= 20º). Additionally, the flow separation is limited to the small area in the TE, and the flow is attached over the SS for AOA lower than 20º for both cases.

At AOA = 25º, the flow separates over the SS of the 40º lambda wing due to the high wing loading at increased AOA. The 40º lambda wing stalls and it is corroborated in Figure 5 with a drop in the lift value. On the contrary, the 65º/40º lambda wing has attached flow, and the stall inception was delayed due to the reduced wing loading.

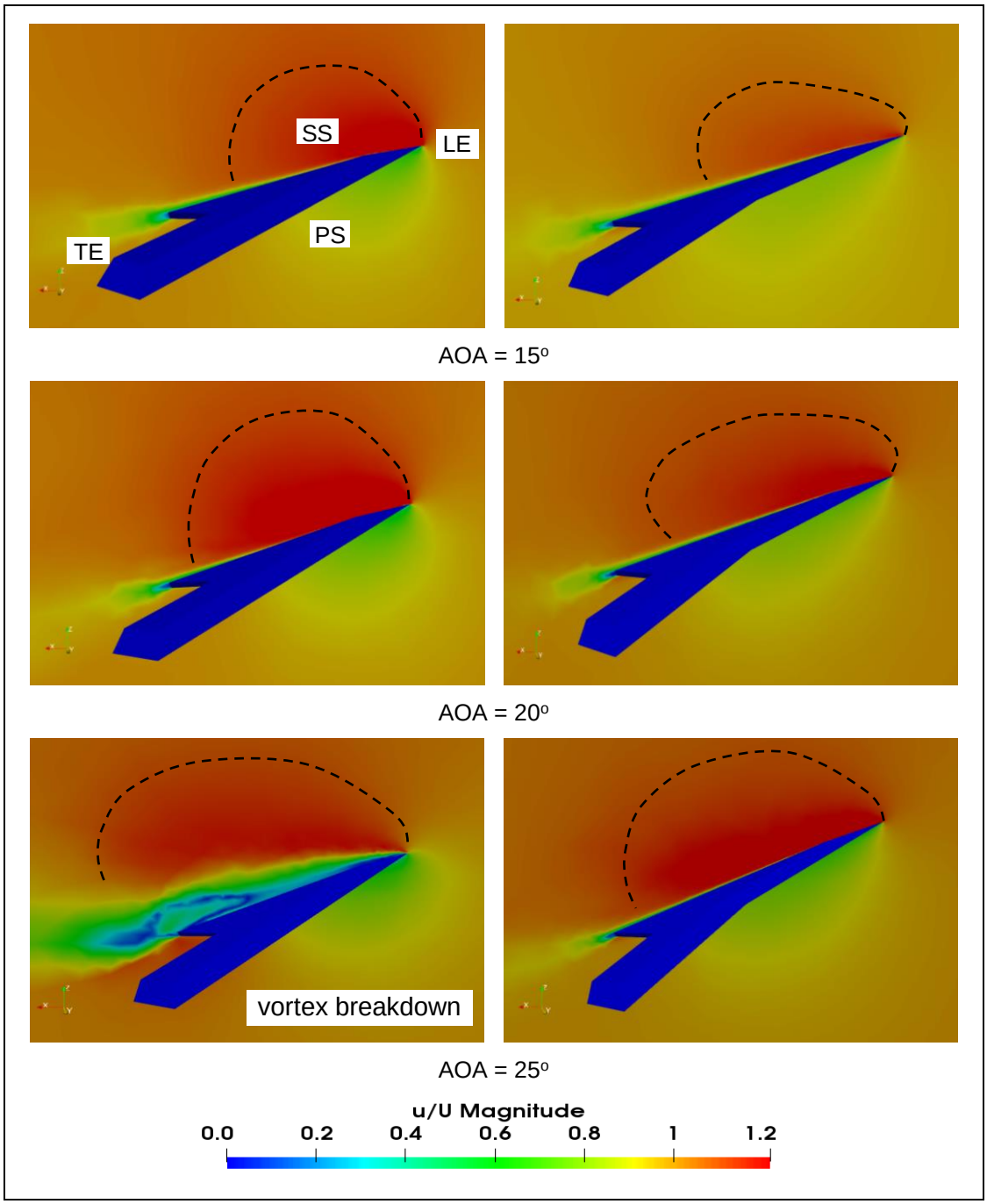

Figure 7: Non-dimensional velocity magnitude of 40º and 65º/40º lambda wings

As discussed in Figures 6 and 7, the velocity magnitude of the vortex flow is greater than the far-field velocity, which increases significantly because of a favorable pressure gradient through the vortex region. However, at 25º AOA (Figure 7), the 40º lambda wing exhibits vortex breakdown because of the low total pressure and severe adverse pressure gradient through the vortex region [Lambourne and Bryer, 1961]. Consequently, the velocity magnitude through the vortex flow is lower than the free stream velocity (Figure 8). As shown in figure 8, after vortex breakdown, the flow separates from the LE and engulfs the SS.

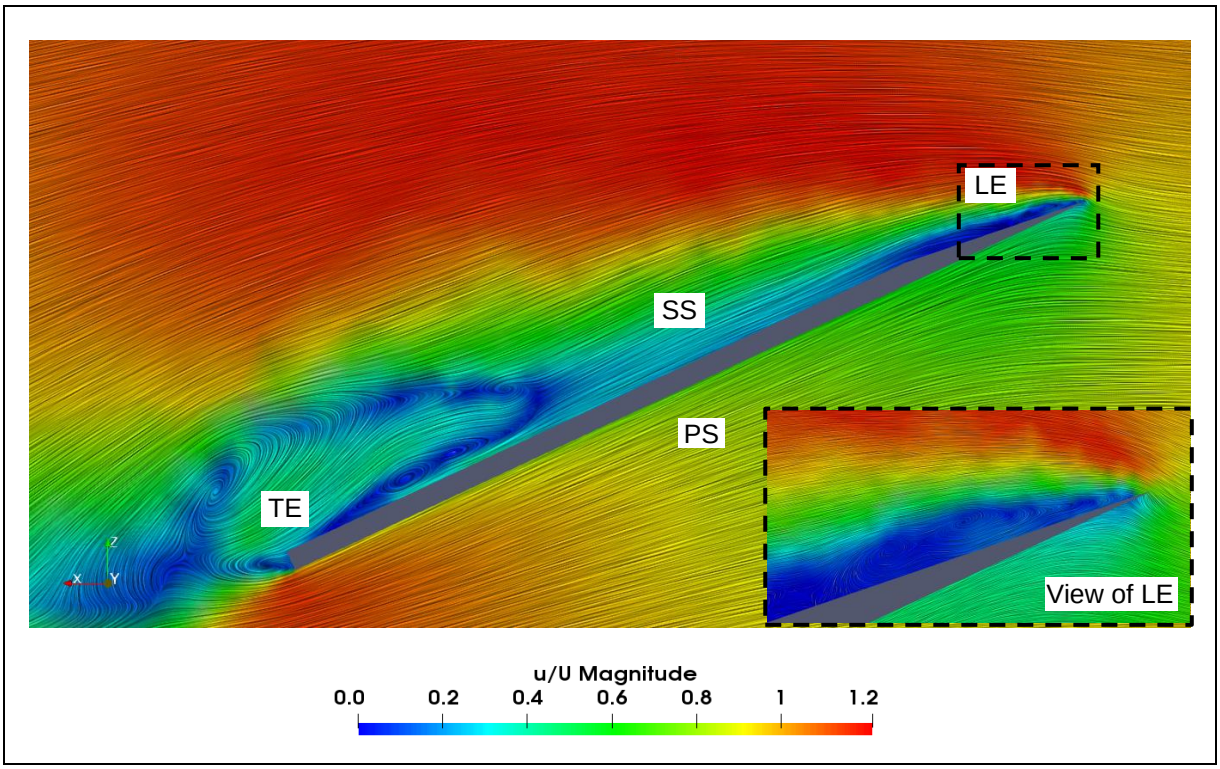

Figure 8: Streamlines visualization of vortex breakdown for 40º Lambda wing at AOA = 25º

The vortices and separated regions are of substantial interest in aerodynamics due to their influences on lift and drag behavior. The flow field around the four configurations was visualized employing pressure distribution and wall shear streamlines to understand the developing flow, attachment and separation, and vortex breakdown with increasing AOA (Figure 9 and 10). The vortex and separation/attachment have been analyzed using critical points such as nodes, foci, and saddles. Additionally, the bifurcation lines that are related to flow attachment (positive or diverging) and separation (negative or converging) have also been included.

Figure 9 illustrates static pressure distribution with wall shear streamlines at 15º, 20º, and 25º AOA for the 65º and 65º/40º delta wings. As evident from the figure, with an increase in AOA, the size and strength of the vortex increase up to the critical AOA. As the AOA increases, the primary attachment lines shift towards the wing inboard for both cases. At a higher AOA, the primary vortex grows radially along with the downstream, which results in the expansion of primary vortex cores. The secondary vortex that has the direction of rotation opposite to the primary vortex is formed underneath the primary vortex. The flow separation is restricted to the TE regions for both wing models, and it is relatively more pronounced in the 65º/40º delta wing compared to the 65º delta wing. Additionally, the vortex breakdown is not observed for both cases, and it corresponds to the results shown in Figure 6.

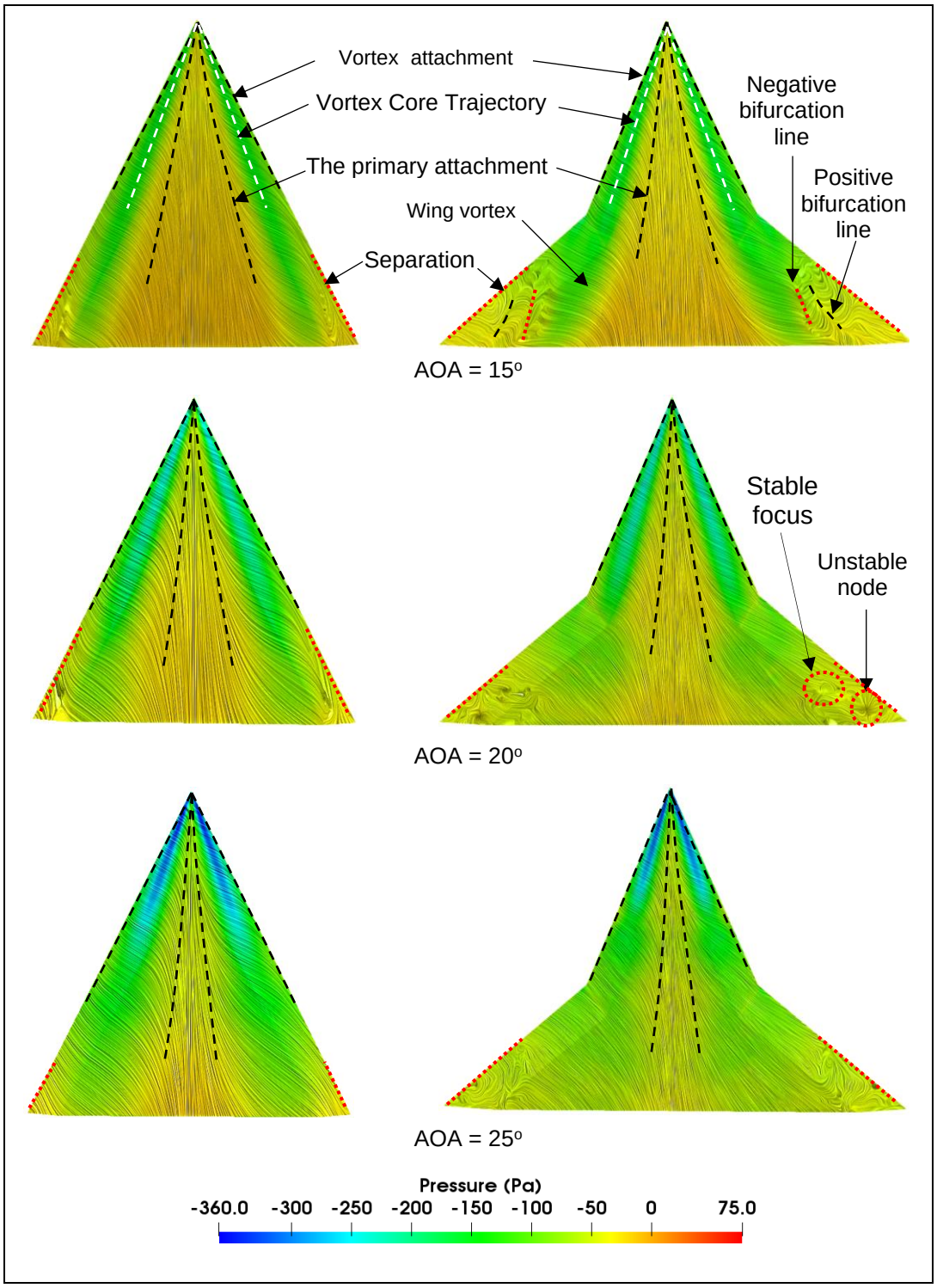

Figure 9: Pressure distribution and wall shear streamlines on the suction surface of 65º and 65º/40º delta wings

The static pressure distribution with wall shear streamlines at 15º, 20º, and 25º AOA for the 40º and 65º/40º lambda wing models is shown in Figure 10. As the AOA increases, the primary attachment lines move towards the wing inboard direction, and this flow behavior of the lambda wings is similar to the delta wing cases (up to critical AOA). As shown in the figure, this phenomenon is more pronounced in the 40º lambda wing compared to the 65º/40º lambda wing. With a further increase in AOA (= 25º), the vortex breakdown occurs for the 40º lambda wing, whereas it is stable for the 65º/40º lambda wing case, and this corroborates with the findings shown in Figures 5 and 7.

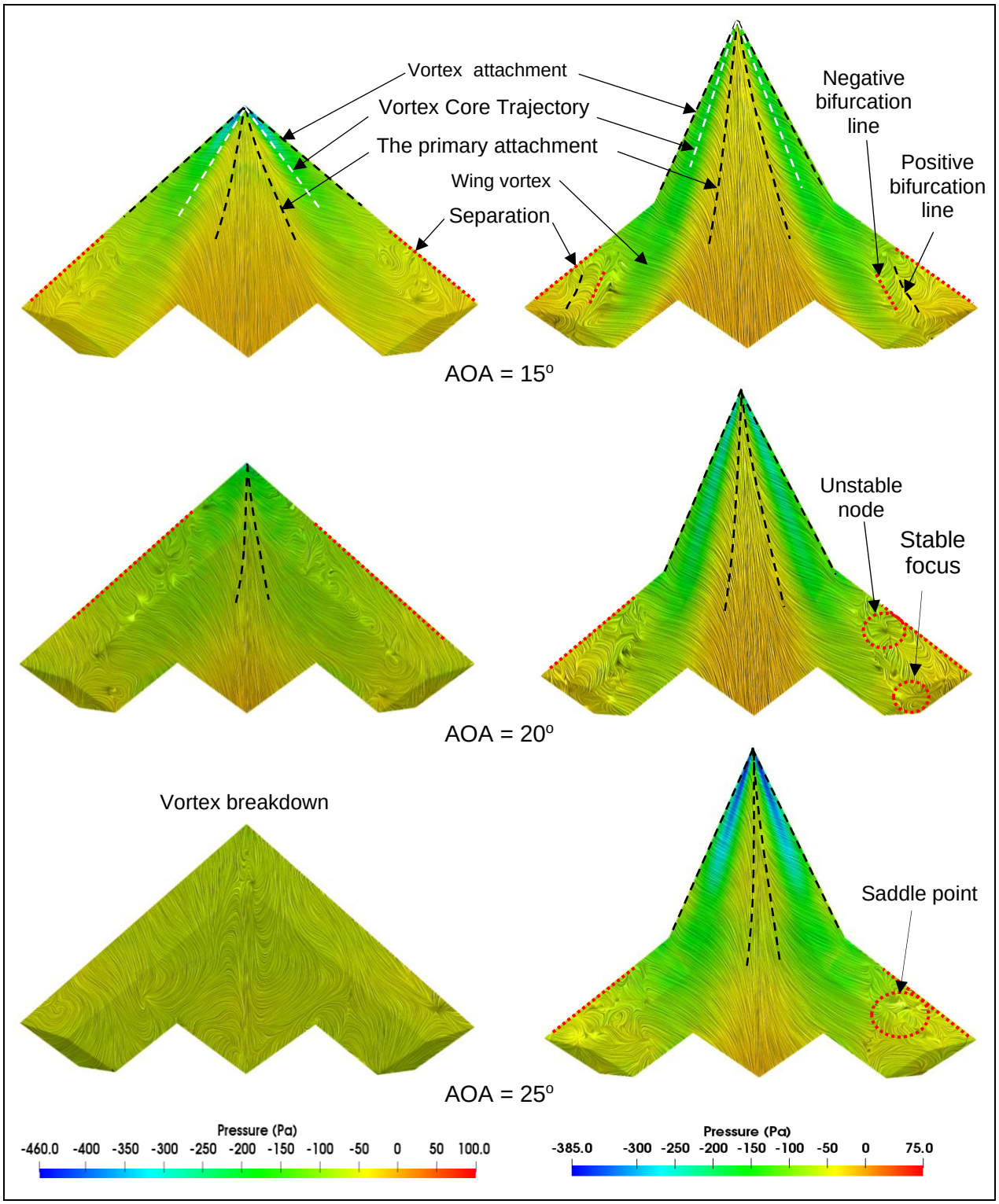

Figure 10: Pressure distribution and wall shear streamlines on the suction surface of 40° and 65°/40° lambda wings

Generally, the vortex breakdown occurs due to the severe adverse pressure gradient and the external flow disturbances. The aerodynamic characteristics of flying-wing configurations depend on the LE sweep angle, and by increasing the sweep angle up to 65°, the stall inception can be delayed. Likewise, the lift was increased, and the peak value shifts towards the higher AOA value. On the other hand, the highly swept flying wings contribute to separated-vortex flow over these wings. As the AOA increases, the departure to the outboard wing section becomes more severe.

CONCLUSION

This study numerically investigated the generic UCAV wings to predict the aerodynamic characteristics at moderate to high AOA. The open-source computational fluid dynamics code OpenFOAM 5.0 is used for the simulations, and the experimental data gathered from the open literature was used to validate the present numerical results. The important conclusions are listed below:

- The present numerical results match well with the experimental data for the lambda wing configurations; in contrast, the delta wing cases show advanced stalls at higher AOA values.

- The LE sweep angle critically influences the lift and stall characteristics of the wing models. The wing with increased sweep angle up to 65° exhibits delayed stall.

- The analyses of wall shear streamlines show the inboard movement of the primary attachment lines with the increase in AOA, and it vanishes at critical AOA due to stall inception.

- Based on the present numerical study, future planned research investigates the flow control mechanism for different UCAV wing configurations and flight conditions to delay the vortex breakdown and improve the vortex lift envelop significantly.

References

Abd Halim, K., and Mat, S., (2015) *Computational fluid dynamic on double delta wing,* Journal of Aeronautical -Science and Engineering, Vol.2, May 20, 2015.

Ali, U., and Chadwick, E., (2016) *Flow control and high-lift performance for flying-wing unmanned combat air vehicle configurations by inserting slots,* Int. Jnl. of Multiphysics Volume 10, 2016

Hövelmann, A., (2016) *Analysis and control of partly-developed leading-edge vortices*, Technical University of Munich, Ph.D. thesis

Al-Garni, A., Saeed, F., and Al-Garni, A., (2008) *Experimental and numerical ınvestigation of 65 degree delta and 65/40 degree double-delta wings*, Journal of Aircraft Vol 45, No. 1, January–February 2008

Ashton, N., Unterlechner, P., and Blacha, T., (2018) *Assessing the sensitivity of hybrid RANS-LES simulations to mesh resolution, numerical schemes and turbulence modeling within an industrial CFD process*, SAE Technical Paper 2018-01-0709.

Canpolat C., Yayla S., Sahin B. and Akilli H. (2012) *Observation of the vortical flow over a yawed delta wing*, Journal of Aerospace Engineering/ Volume 25 Issue 4

Earnshaw, P., (1961) *An experimental investigation of the structure of a leading-edge vortex*, Aeronautical Research Council Reports and Memoranda, No. 3281, 1961

Frink, N., (2010) *Strategy for dynamic CFD simulations on SACCON configuration*, AIAA 2010-4559, Jun 2010

Greenshields, C., (2015) *OpenFOAM user guide version 5.0*. OpenFOAM Foundation Ltd.

Huber, K., Schütte A., and Rein M., (2012) *Numerical ınvestigation of the aerodynamic properties of a flying wing configuration*, 30th AIAA Applied Aerodynamics Conference 25 - 28 June 2012, New Orleans, Louisiana

Lambourne, N., and Bryer, D., (1959) *Some measurements in the vortex flow generated by a sharp leading edge having 65 degrees sweep*, Aeronautical Research Council Current Papers, No. 477, 1959

Lambourne, N., and Bryer, D., (1961) *The bursting of leading-edge vortices: some observations and discussion of the phenomenon*, Aeronautical Research Council Reports and Memoranda, No. 3282.

Manshadi, M., Eilbeigi, M., Mohammad M., Zadeh, M., and Vaziry, M., (2016) *Experimental study of flow field distribution over a generic cranked double delta wing*, Chinese Journal of Aeronautics, (2016), 29, (5): 1196 - 1204

Patel, M., Terry Ng, T., Vasudevan, S., Corke, T., and Chuan, H., (2007) *Plasma Actuators for Hingeless Aerodynamic Control of an Unmanned Air Vehicle*, Journal OF Aircraft Vol 44, No. 4, July–August 2007

Petterson, K., (2006) *CFD Analysis of the low-speed aerodynamic characteristics of a ucav*, 44th AIAA Aerospace Sciences Meeting and Exhibit, 2006.

Polhamus, E., (1971) *Predictions of vortex-lift characteristics by a leading edge suction analogy*, Journal of Aircraft, Vol. 8, No. 4, Apr. 1971, pp. 194-198.

Puckett, A. and Stewart, H., (1947) *Aerodynamic performance of delta wings at supersonic speeds*, Journal of the Aeronautical Sciences, Vol. 14, No. 10, pp. 567-578, Oct. 1947. 4

Shima, H., and Parka, S., (2013) *Low-speed wind-tunnel test results of a BWB-UCAV model*, 7th Asian-Pacific Conference on Aerospace Technology and Science, 7th APCATS 2013

Sidorenko, A., Budovskiy, A., Maslov, A., Postnikov B., Zanin, B., Zverkov I., and Kozlov, V., (2013) *Plasma control of vortex flow on a delta wing at high angles of attack,* Exp Fluids, 2013 54:1585.

Verhaagen, N., (2011) *Flow over 50^o Delta Wings with Different Leading-Edge Radii*, 49th AIAA Aerospace Sciences Meeting including the New Horizons Forum and Aerospace Exposition 4 - 7 January 2011, Orlando, Florida

Wang, J., and Zhan, J., (2005) *New Pair of Leading-Edge Vortex Structure for Flow over Delta Wing*, JOURNAL OF AIRCRAFT Vol 42, No. 3, May–June 2005

Wibowo S., Sutrısno and Rohmat, T., (2018) *An Evaluatıon of Turbulence Model for Vortex Breakdown Detectıon over Delta Wing*, Archive of Mechanical Engineering; 2018; vol. 65; No 3; 399-415 3.

Zhang S., Jaworski, A., McParlin, S., and Turner, T., (2019) *Experimental investigation of the flow structures over a 40° swept wing*, pp 40–54. Royal Aeronautical Society.